LETTER

doi:10.1038/nature11097

Recent Northern Hemisphere tropical expansion primarily driven by black carbon and tropospheric ozone

Robert J. Allen[1], Steven C. Sherwood[2], Joel R. Norris[3] & Charles S. Zender[4]

Observational analyses have shown the width of the tropical belt increasing in recent decades as the world has warmed[1]. This expansion is important because it is associated with shifts in large-scale atmospheric circulation[2–4] and major climate zones[5,6]. Although recent studies have attributed tropical expansion in the Southern Hemisphere to ozone depletion[7–10], the drivers of Northern Hemisphere expansion are not well known and the expansion has not so far been reproduced by climate models[11]. Here we use a climate model with detailed aerosol physics to show that increases in heterogeneous warming agents—including black carbon aerosols and tropospheric ozone—are noticeably better than greenhouse gases at driving expansion, and can account for the observed summertime maximum in tropical expansion. Mechanistically, atmospheric heating from black carbon and tropospheric ozone has occurred at the mid-latitudes, generating a poleward shift of the tropospheric jet[12], thereby relocating the main division between tropical and temperate air masses. Although we still underestimate tropical expansion, the true aerosol forcing is poorly known and could also be underestimated. Thus, although the insensitivity of models needs further investigation, black carbon and tropospheric ozone, both of which are strongly influenced by human activities, are the most likely causes of observed Northern Hemisphere tropical expansion.

Recent observational analyses show that the tropics have widened by 2°–5° latitude since 1979 (ref. 1). This evidence is based on several metrics, including a poleward shift of the Hadley cell[2], subtropical dry zones[5], and extratropical storm tracks[6]. A more recent estimate of the tropospheric jet shift[4], based on satellite-derived temperatures, suggests a smaller rate of expansion of 1.6°.

Tropical expansion occurs in model simulations forced by increasing greenhouse gases, thus suggesting a likely cause[1,13,14]. Model-predicted expansion rates, however, are significantly less than those observed[11]. This discrepancy may be related to the relatively short observational record, the large natural variability of some expansion metrics, or model deficiencies.

Several recent studies have focused on tropical expansion in the Southern Hemisphere, and the important contribution of stratospheric ozone depletion[7–10]. Less has been said about the causes of Northern Hemisphere expansion. Recent equilibrium simulations with atmospheric general circulation models have shown that direct heating of the troposphere, such as that caused by absorbing aerosols or tropospheric ozone, can drive expansion[15]. Although indirect aerosol effects may also be important and could yield the opposite response[16], they may be significantly overestimated in current general circulation models[17] and in any case they mainly cool the surface rather than the atmosphere.

Owing to increased combustion of fossil fuels and biofuels, black carbon aerosols have increased substantially over much of the Northern Hemisphere during the last few decades, particularly over southeast Asia, while decreasing over much of Europe (Fig. 1). Despite the geographically heterogeneous evolution, black carbon has

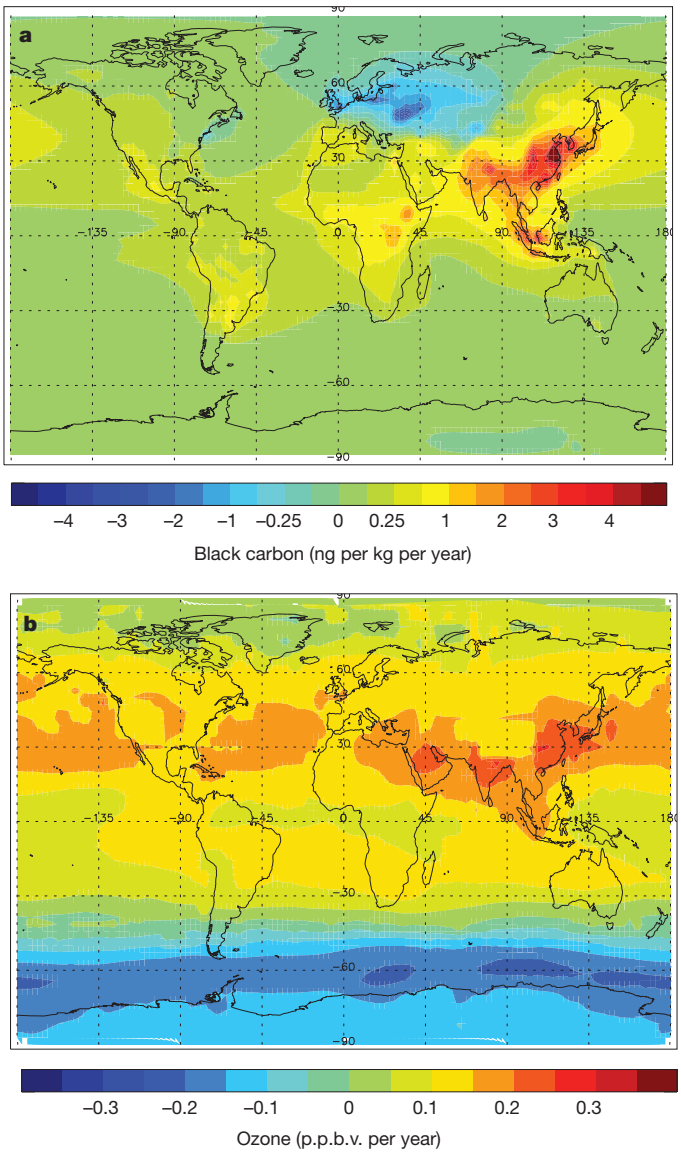

Figure 1 | 1970–2009 annual mean tropospheric trends. **a**, Black carbon; **b**, Ozone. p.p.b.v., parts per billion by volume. Black carbon concentration trends include hydrophobic and hydrophilic black carbon and are based on CAM simulations using CMIP5 black carbon emissions. Ozone trends come directly from the CMIP5 forcing data set.

[1]Department of Earth Sciences, University of California, Riverside 92521, USA. [2]Climate Change Research Centre and ARC Centre of Excellence for Climate Systems Science, University of New South Wales, Sydney 2052, Australia. [3]Scripps Institution of Oceanography, University of California, San Diego 92093, California, USA. [4]Earth System Science, University of California, Irvine 92697, California, USA.

increased monotonically since 1970 on average in the low and mid-latitudes, including the band 30°–50° N (Supplementary Figs 1–2), where recent studies show that heating can displace the tropical edge[12]. The same is true of tropospheric ozone, another indirect byproduct of combustion. Here, we investigate the transient effects of these atmospheric warming agents on Northern Hemisphere tropical width.

We quantify tropical width using a variety of metrics[5,11]: (1) the latitude of the tropospheric zonal wind maxima (JET); (2) the latitude where the Mean Meridional Circulation (MMC) at 500 hPa becomes zero on the poleward side of the subtropical maximum; (3) the latitude where precipitation minus evaporation (P − E) becomes zero on the poleward side of the subtropical minimum; (4) the latitude of the subtropical precipitation minimum (PMIN); and (5) the latitude of the subtropical cloud cover minimum over oceans (CMIN). To obtain an overall measure of tropical expansion, we also average the trends of all five metrics into a combined metric called 'ALL'. Expansion figures quoted in the text will be based on ALL unless otherwise specified.

Figure 2 compares the annual-mean poleward displacement of each metric, with 2σ uncertainty, between observations and a much-studied set of twentieth-century (Coupled Model Intercomparison Project version 3, CMIP3) climate simulations (Supplementary Table 1) for the period 1979–99, for which both observations and simulations are available. All observed metrics show poleward displacement of the Northern Hemisphere tropical boundary by 0.2°–0.75° per decade. Although the JET and PMIN displacements are not significant at the 95% confidence level, the others are, and the combined metric ALL shows significant poleward displacement of 0.33° ± 0.12° per decade.

As shown previously[11], the CMIP3 models underestimate Northern Hemisphere expansion. However, we note that this failure is more evident in models that lack time-varying black carbon or ozone, wherein four of the five metrics actually move in the wrong direction. In models that do include one or both forcings, poleward displacement is robust across most indicators. In those with both forcings, ALL shows 0.14 ± 0.06° per decade—about half what is observed and significantly more than in models not including black carbon and ozone forcing (non-BC/O_3).

Expansion rates vary by season (Fig. 2, bottom). In the Northern Hemisphere, observed expansion is strongest in June–August (JJA) and September–November (SON) at 0.53° per decade and 0.58° per decade, respectively. Non-BC/O_3 CMIP3 models significantly underestimate expansion in these seasons. Models that include ozone, however, and those also including black carbon, simulate more expansion in JJA and SON. The impact of both forcings (BC + O_3), that is, the difference relative to non-BC/O_3, is greatest in JJA (0.24° per decade) followed by SON (0.20° per decade) and March–May (MAM) (0.15° per decade), with the smallest difference in December–February (DJF) (0.07° per decade). Such a seasonal cycle is similar to that of the observed trend, although expansion overall is still too small even in the BC + O_3 models. The impact of these forcings becomes more statistically significant in the models when examining a longer time period, 1970–1999 (Supplementary Fig. 3).

The preceding results are based on a relatively short time period, are probably affected by differences between the models that used different forcings, and were based on relatively crude aerosol treatments. We therefore conduct a suite of longer (1970–2009) simulations with a single climate model, the Community Atmosphere Model version 3 (CAM3)[18] of the National Center for Atmospheric Research (NCAR), equipped with new aerosol physics. We isolate the impact of a given forcing agent by comparing model runs with and without that agent.

The annual-mean observed displacement over 1979–2009, 0.38 ± 0.11° per decade, is about 15% stronger than for the shorter period and has approximately the same seasonal cycle (Fig. 3). The CAM 1979–2009, CAM 1970–2009, and CMIP3 BC + O_3 1979–1999 runs all produce similar counterpart expansions of about 0.14° per decade, with similar seasonal cycles. Therefore none of the important results are sensitive to the observing period.

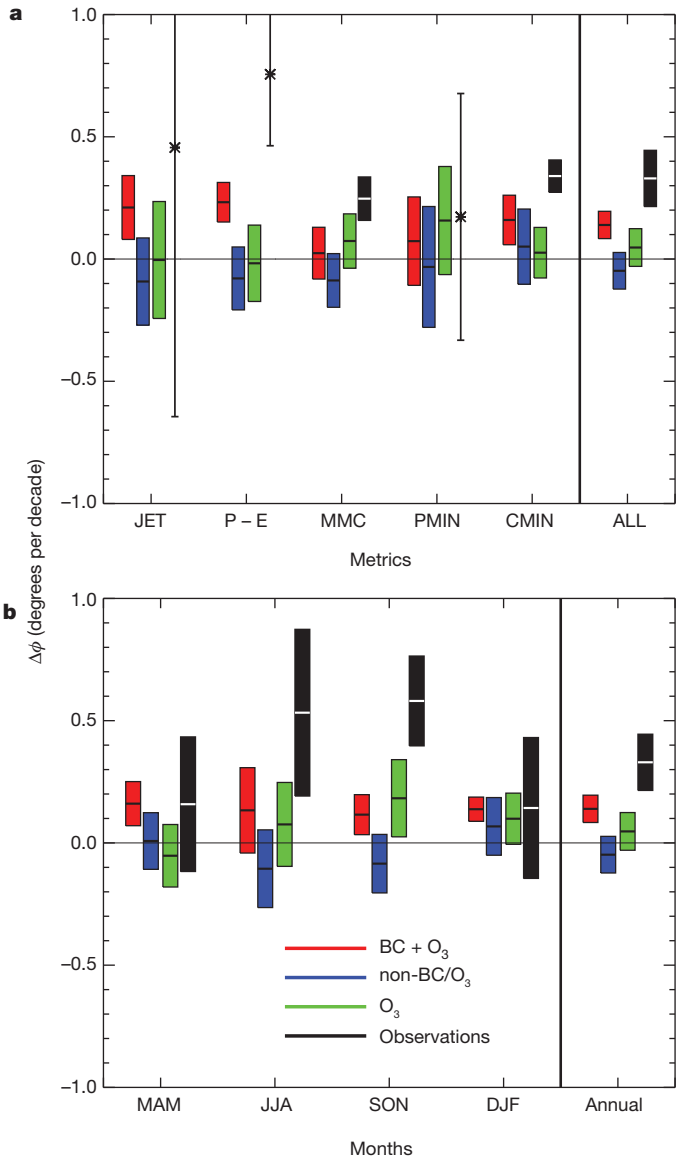

Figure 2 | Observed and modelled 1979–1999 Northern Hemisphere tropical expansion based on five metrics. **a**, Annual mean poleward displacement of each metric, as well as the combined ALL metric. **b**, Poleward displacement by season, based on ALL. CMIP3 models are grouped into nine that included time-varying black carbon and ozone (red); three that included time-varying ozone only (green); and six that included neither time-varying black carbon nor ozone (blue). Boxes show the mean response within each group (centre line) and its 2σ uncertainty. Observations are in black. In the case of one observational data set, trend uncertainty (whiskers) is estimated as the 95% confidence level according to a standard *t*-test.

These CAM simulations confirm the important role of time-varying black carbon and ozone in driving simulated expansion. In the non-BC/O_3 run, annual-mean expansion dropped to 0.04 ± 0.03° per decade, or about one-third of that with all forcings. Little if any of this is due to stratospheric ozone, given that almost the same result (0.06 ± 0.04° per decade) is obtained in the non-BC/tO_3 run, where tO_3 is tropospheric ozone. Although the latter result is not quite significantly different from the all-forcings response over 1979–2009, it is significantly different over the longer time period, and is robust across metrics (Supplementary Fig. 4). Moreover, as seen in the CMIP3 simulations, BC + tO_3 produces a much more realistic warm-season trend maximum; the JJA and MAM trend increases are statistically significant .

Black carbon and tropospheric ozone are negligible drivers of Southern Hemisphere expansion (Supplementary Fig. 5). Instead we

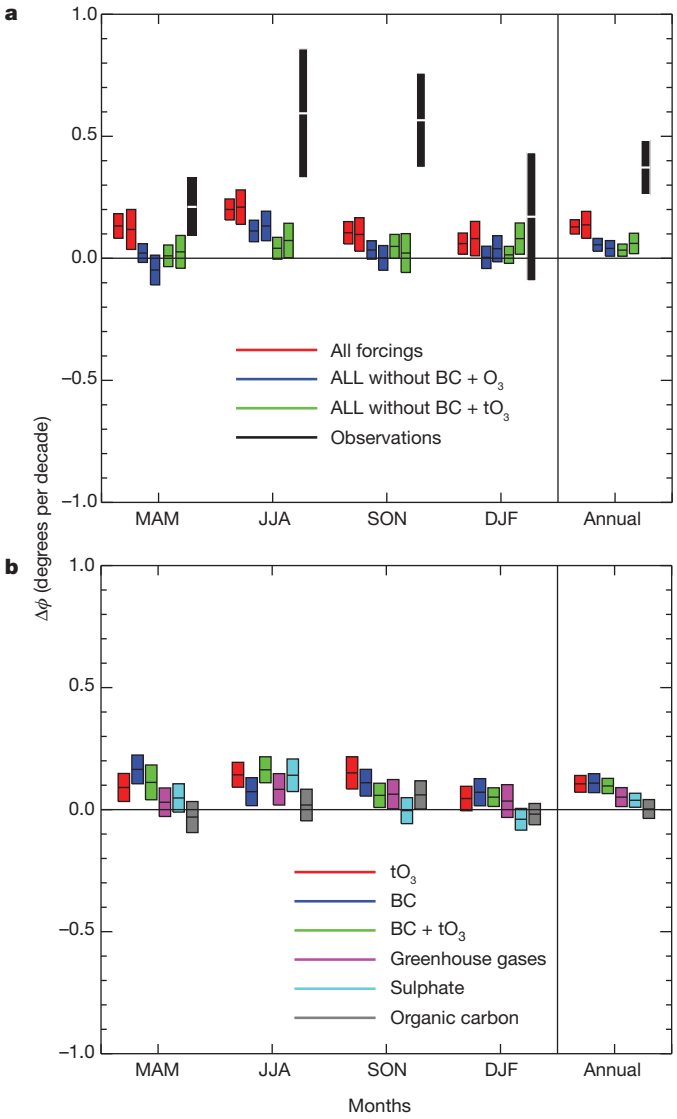

Figure 3 | Northern Hemisphere seasonal tropical expansion based on the combined ALL metric. **a**, CAM simulations for all forcings (red), all forcings except black carbon and ozone (blue); and all forcings except black carbon and tropospheric ozone (green). The first box in each like-coloured pair represents 1970–2009; the second box in each like-coloured pair represents 1979–2009. Observations (black) for 1979–2009 are also included. **b**, CAM individual forcing experiments for 1970–2009 showing the difference between the all forcings experiment and all forcings without tropospheric ozone (red), black carbon (blue), black carbon and tropospheric ozone (green), greenhouse gases (purple), sulphate (light blue) and organic carbon (grey). Boxes show the mean response (centre line) and its 2σ uncertainty.

find, as have previous studies[7–10], that stratospheric ozone depletion is the main driver there, particularly during the peak DJF expansion season.

We explored the role of various forcings more thoroughly by conducting additional ten-ensemble member simulations with CAM, individually omitting each of black carbon, tropospheric ozone, greenhouse gases, and the scattering aerosols—sulphate and organic carbon (Fig. 3b). In most seasons, greenhouse gases and heterogeneous warming agents (that is, black carbon and tropospheric ozone) push the Northern Hemisphere tropical boundary poleward. Over the year, greenhouse gases yield about 0.05° per decade, which is only significant for the longest time period, 1970–2009. Either tropospheric ozone, black carbon or their combination (BC + tO_3) each cause roughly twice this much expansion, ranging from 0.07° to 0.12° per decade, which is significant for both time periods (Supplementary Fig. 6 shows 1979–2009). The combined impact of black and organic carbon (which are generally emitted together) also falls in this range, showing that little of the expansion from black carbon is offset by organic carbon, which is non-absorbing. These results are again qualitatively robust across individual metrics, although less statistically significant (Supplementary Fig. 7). Each of the heterogeneous warming agents produces a more realistic seasonal trend cycle than do greenhouse gases. Decreases in scattering aerosols (due to declining mid-latitude sulphate) have not significantly contributed to Northern Hemisphere tropical expansion except during JJA, the time of maximum solar insolation.

We relate tropical expansion to a temperature index that compares mid-latitude tropospheric warming to that at other latitudes[12]. Warming of mid-latitudes relative to others displaces the maximum meridional climatological temperature gradient poleward. Geostrophic adjustment to this perturbed temperature gradient also implies a poleward shift of the tropospheric jet[12].

We consider a quantity called the 'expansion index': $2 \times \Delta T_{30-60} - (\Delta T_{0-30} + \Delta T_{60-90})$, where ΔT is the log-pressure (850–300 hPa) area-weighted temperature response in low (0°–30°), mid- (30°–60°), and high (60°–90°) latitudes[12]. As the expansion index becomes more positive, mid-latitude warming amplification dominates, and we expect more tropical expansion. Similarly, as the expansion index becomes less positive, mid-latitude cooling amplification dominates, and we expect less tropical expansion.

The above relationship helps to explain why black carbon and tropospheric ozone drive Northern Hemisphere tropical expansion (Supplementary Information and Supplementary Figs 8–14). Both agents heat primarily within the 30°–55° N latitude range. Although dynamical responses can cause the geographical patterns of applied heating and resulting warming to be quite different, in the zonal mean, mid-latitude heat input does appear to produce warming at roughly the heated latitudes[12], consistent with our results. Experiments with an alternative general circulation model, the Geophysical Fluid Dynamics Laboratory (GFDL) atmospheric model AM2.1 (ref. 19 and Supplementary Information), increase our confidence that this response to mid-latitude heating, and black carbon and tropospheric ozone in particular, is robust across different climate models, as well as different aerosol and ozone forcings.

This relationship also explains the seasonal cycle of the response, because both black carbon and tropospheric ozone warm primarily by absorbing solar radiation, which is far more abundant during summer. In our CAM simulations, atmospheric solar absorption by black carbon in the Northern Hemisphere mid-latitudes increases by more than a factor of three from DJF to JJA, 0.76 W m^{-2} versus 2.63 W m^{-2}. This results in about 0.05 K per decade more tropospheric warming in the Northern Hemisphere mid-latitudes during JJA compared to DJF. A similar variation results from tropospheric ozone (Supplementary Fig. 15).

Figure 4 quantifies the relationship between annual mean Northern Hemisphere tropical expansion and expansion index for 1970–2009. Climate forcing agents that yield a positive expansion index also yield a positive (poleward) displacement for most metrics, and vice versa. The corresponding correlation coefficient, over all experiments and metrics is 0.66, significant at the 99% confidence level. Correlations for the individual metrics are 0.86 for JET; 0.62 for P − E; 0.89 for MMC; 0.68 for PMIN; and 0.16 for CMIN.

Our analysis strongly suggests that recent Northern Hemisphere tropical expansion is driven mainly by black carbon and tropospheric ozone, with greenhouse gases playing a smaller part. Compared to observations, the magnitude of the simulated change is underestimated. This could be related to the aforementioned caveats with the observations, model deficiencies, or deficient black carbon aerosol forcing. The average top-of-the-atmosphere black carbon radiative forcing is 0.35 W m^{-2} for CMIP3 models[20], 0.43 W m^{-2} in our CAM simulations, and was reported as 0.25 W m^{-2} in a third suite of relatively

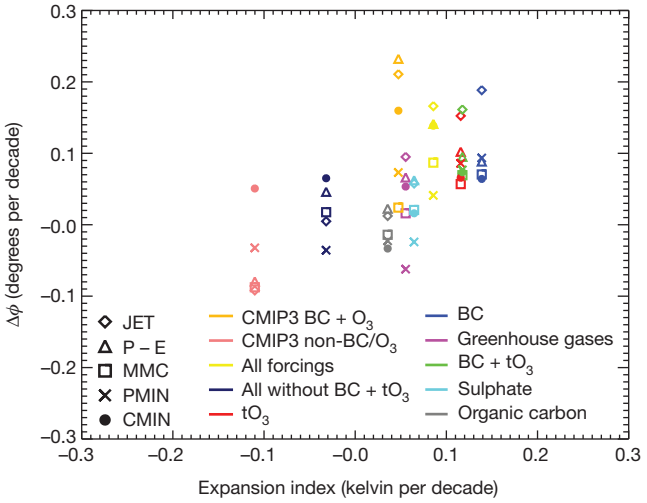

Figure 4 | Northern Hemisphere 1970–2009 annual mean tropical expansion for each metric versus the expansion index for CAM simulations. Also included are CMIP3 results from 1979–1999, stratified by BC + O_3 (orange) versus non-BC/O_3 (pink) models.

sophisticated models from the Aerosol Comparisons between Observations and Models (AeroCom)[21] project. However, recent observationally constrained estimates[22] range from 0.4 W m^{-2} to 1.2 W m^{-2}. Although others have inferred a similarly large magnitude of black carbon forcing[23,24], we emphasize that uncertainties still exist. It is also possible that the increase in black carbon emissions—particularly in southeast Asia—is underestimated, as has been inferred with CMIP3 aerosol emission inventories[25].

The upper end of the observed range of black carbon would reconcile the 2.5 factor shortfall in all-forcings expansion relative to observations, if responses varied linearly with forcing. However, our results show that responses are not always linear, and it still seems likely that models are insufficiently sensitive to these forcings. As long as this insensitivity applies equally to different forcings, our results point to anthropogenic pollutants other than CO_2 rather than global warming as the culprit in recent Northern Hemisphere tropical expansion. Emission controls on black carbon and ozone precursors would thus not only help mitigate global warming and improve human health[26], but could lessen the regional impacts of changes in large-scale Northern Hemisphere atmospheric circulation.

METHODS SUMMARY

CAM was run at T42 resolution coupled to the Community Land Model (CLM) version 3, a slab ocean-thermodynamic sea ice model, and the Snow, ICe and Aerosol Radiative (SNICAR) model[27,28] for the period 1970–2009. In addition to the usual natural forcings, our runs included radiatively active black carbon in the atmosphere and snow and an enhancement factor of 1.5 for solar absorption by coated hydrophilic particles[27,29]. Aerosol indirect effects were not included. Time-varying forcing followed the newly developed CMIP5 data set, including estimated concentrations of greenhouse gases and primary emissions of sulphur dioxide, black and organic carbon. Post-2005 emissions were derived from the average of the four representative concentration pathways and data are linearly interpolated to annual resolution. We show results from a ten-member ensemble with each member integrated from an independent initial condition based on a 30-year control simulation with constant 1970 forcing. Analysing the correlation between individual ensemble members' time series of several tropical expansion metrics supported the independence of each realization, because correlations on both annual and longer timescales ranged from −0.01 to 0.13.

Changes in tropical width were estimated by taking a least-squares trend of the seasonal or annual mean time series of each metric. The median of pairwise slopes regression yielded similar results. When multiple realizations (or observational data sets for a given metric) were available, trend uncertainty was estimated from the multiple realizations, as twice the standard error, $2 \times \frac{\sigma}{\sqrt{n}}$, where σ is the standard deviation of the trends and n is the number of trends. In the case of one observational data set, trend uncertainty was estimated as the 95% confidence level according to a standard t-test[30].

Full Methods and any associated references are available in the online version of the paper at www.nature.com/nature.

Received 16 December 2011; accepted 29 March 2012.

1. Seidel, D. J., Fu, Q., Randel, W. J. & Reichler, T. J. Widening of the tropical belt in a changing climate. *Nature Geosci.* **1,** 21–24 (2008).
2. Hu, Y. & Fu, Q. Observed poleward expansion of the Hadley circulation since 1979. *Atmos. Chem. Phys.* **7,** 5229–5236 (2007).
3. Fu, Q., Johanson, C. M., Wallace, J. M. & Reichler, T. Enhanced mid-latitude tropospheric warming in satellite measurements. *Science* **312,** 1179 (2006).
4. Fu, Q. & Lin, P. Poleward shift of subtropical jets inferred from satellite-observed lower stratospheric temperatures. *J. Clim.* **24,** 5597–5603 (2011).
5. Zhou, Y. P., Xu, K.-M., Sud, Y. C. & Betts, A. K. Recent trends of the tropical hydrological cycle inferred from Global Precipitation Climatology Project and International Satellite Cloud Climatology Project data. *J. Geophys. Res.* **116,** D09101 (2011).
6. Bender, F., Ramanathan, V. & Tselioudis, G. Changes in extratropical storm track cloudiness 1983–2008: observational support for a poleward shift. *Clim. Dyn.* http://dx.doi.org/10.1007/s00382-011-1065-6 (2011).
7. Son, S.-W., Tandon, L. M., Polvani, L. M. & Waugh, D. W. Ozone hole and Southern Hemisphere climate change. *Geophys. Res. Lett.* **36,** L15705 (2009).
8. Polvani, L. M., Waugh, D. W., Correa, G. J. P. & Son, S.-W. Stratospheric ozone depletion: the main driver of twentieth-century atmospheric circulation changes in the Southern Hemisphere. *J. Clim.* **24,** 795–812 (2011).
9. Son, S.-W. *et al.* Impact of stratospheric ozone on Southern Hemisphere circulation change: a multimodel assessment. *J. Geophys. Res.* **115,** D00M07 (2010).
10. Kang, S. M., Polvani, L. M., Fyfe, J. C. & Sigmond, M. Impact of polar ozone depletion on subtropical precipitation. *Science* **332,** 951–954 (2011).
11. Johanson, C. M. & Fu, Q. Hadley cell widening: model simulations versus observations. *J. Clim.* **22,** 2713–2725 (2009).
12. Allen, R. J., Sherwood, S. C., Norris, J. R. & Zender, C. S. The equilibrium response to idealized thermal forcings in a comprehensive GCM: implications for recent tropical expansion. *Atmos. Chem. Phys. Discuss.* **11,** 31643–31688 (2011).
13. Lu, J., Vecchi, G. A. & Reichler, T. Expansion of the Hadley cell under global warming. *Geophys. Res. Lett.* **34,** L06805 (2007).
14. Lu, J., Deser, C. & Reichler, T. Cause of the widening of the tropical belt since 1958. *Geophys. Res. Lett.* **36,** L03803 (2009).
15. Allen, R. J. & Sherwood, S. C. The impact of natural versus anthropogenic aerosols on atmospheric circulation in the Community Atmosphere Model. *Clim. Dyn.* **36,** 1959–1978 (2011).
16. Ming, Y., Ramaswamy, V. & Chen, G. A model investigation of aerosol-induced changes in boreal winter extratropical circulation. *J. Clim.* **24,** 6077–6091 (2011).
17. Quaas, J., Boucher, O., Bellouin, N. & Kinne, S. Satellite-based estimate of the direct and indirect aerosol climate forcing. *J. Geophys. Res.* **113,** D05204 (2008).
18. Collins, W. D. *et al. Description of the NCAR Community Atmosphere Model (CAM3).* Technical Report NCAR/TN-464+STR (National Center for Atmospheric Research, 2004).
19. The GFDL Global Atmospheric Model Development Team.. The new GFDL global atmosphere and land model AM2–LM2: evaluation with prescribed SST simulations. *J. Clim.* **17,** 4641–4673 (2004).
20. Forster, P. *et al.* In *Climate Change 2007: The Physical Science Basis. Contribution of Working Group I to the Fourth Assessment Report of the Intergovernmental Panel on Climate Change* (eds Solomon, S. *et al.*) Ch. 2 130–234 (Cambridge University Press, 2007).
21. Schulz, M. *et al.* Radiative forcing by aerosols as derived from the AeroCom present-day and pre-industrial simulations. *Atmos. Chem. Phys.* **6,** 5225–5246 (2006).
22. Ramanathan, V. & Carmichael, G. Global and regional climate changes due to black carbon. *Nature Geosci.* **1,** 221–227 (2008).
23. Sato, M. *et al.* Global atmospheric black carbon inferred from AERONET. *Proc. Natl Acad. Sci. USA* **100,** 6319–6324 (2003).
24. Chung, S. H. & Seinfeld, J. H. Global distribution and climate forcing of carbonaceous aerosols. *J. Geophys. Res.* **107,** D19 (2002).
25. Dwyer, J. G., Norris, J. R. & Ruckstuhl, C. Do climate models reproduce the observed solar dimming and brightening over China and Japan? *J. Geophys. Res.* **115,** D00K08 (2010).
26. Shindell, D. *et al.* Simultaneously mitigating near-term climate change and improving human health and food security. *Science* **335,** 183–189 (2012).
27. Flanner, M. G., Zender, C. S., Randerson, J. T. & Rasch, P. J. Present-day climate forcing and response from black carbon in snow. *J. Geophys. Res.* **112,** D11202 (2007).
28. Flanner, M. G. *et al.* Springtime warming and reduced snow cover from carbonaceous particles. *Atmos. Chem. Phys.* **9,** 2481–2497 (2009).
29. Bond, T. C. & Bergstrom, R. W. Light absorption by carbonaceous aerosols: an investigative review. *Aerosol Sci. Technol.* **40,** 27–67 (2006).
30. Wilks, D. S. *Statistical Methods in the Atmospheric Sciences* (Academic Press, 2006).

Supplementary Information is linked to the online version of the paper at www.nature.com/nature.

Acknowledgements This study was funded by R.J.A.'s University of California at Riverside initial complement. We acknowledge the individual modelling groups, the

Program for Climate Model Diagnosis and Intercomparison and the Working Group on Coupled Modeling of the World Climate Research Programme (WCRP) for their part in making available the WCRP CMIP3 multimodel data set. Support of this data set is provided by the Office of Science, US Department of Energy.

Author Contributions R.J.A. conceived the project, designed the study, carried out all data analysis and wrote the manuscript. S.C.S. advised on methods and interpretation, and assisted in the writing of the manuscript. J.N. provided homogenized cloud data and assisted in experimental design. C.S.Z. assisted with CAM experiments, including the SNICAR model.

Author Information Reprints and permissions information is available at www.nature.com/reprints. The authors declare no competing financial interests. Readers are welcome to comment on the online version of this article at www.nature.com/nature. Correspondence and requests for materials should be addressed to R.J.A. (rjallen@ucr.edu).

METHODS

Our black carbon radiative forcing is computed interactively at each time step as the difference in fluxes with all species present and all species except black carbon. Thus, our 0.43 W m^{-2} top-of-the-atmosphere radiative forcing is a measure of the instantaneous forcing, which for aerosols is a close approximation of the (adjusted) radiative forcing used by CMIP3 models. CAM alterations, including the SNICAR model and modification of black carbon optical properties to account for enhanced solar absorption by coated hydrophilic particles, are described elsewhere[27,28].

Observational data comes from several sources, including the Global Precipitation Climatology Project version 2.2 (GPCP)[31] the Integrated Global Radiosonde Archive (IGRA)[32] and five reanalyses[33–37] for MMC calculations. Cloud cover observations, which span July 1983 to June 2008 only, come from two recently homogenized satellite data sets[38] based on the International Satellite Cloud Climatology Project (ISCCP)[39,40] and the Advanced Very High Resolution Radiometer (AVHRR) Pathfinder Atmospheres Extended (PATMOS-x)[41,42]. Our P − E estimate is based on precipitation from GPCP and evaporation from the Woods Hole Oceanographic Institution (WHOI) Objectively Analyzed air-sea Flux (OAFlux) project[43]. Because the WHOI OAFlux data are over ocean only, our P − E estimate is for the global oceans.

For the IGRA jet analysis, monthly mean zonal wind data are used at stations with 75% valid years, where a valid year has four valid seasons and a valid season has two of three valid months. This is required at all tropospheric pressure levels (850 hPa, 700 hPa, 500 hPa, 400 hPa, 300 hPa). To minimize trend errors, we also required a station to possess eight valid years in the first and last decade. Data from both 00Z and 12Z are used. This resulted in 273 12Z and 300 00Z IGRA stations for 1979–1999 and 247 12Z and 281 00Z stations for 1979–2009, most of which are in the Northern Hemisphere. Data are gridded to $5^\circ \times 10^\circ$ resolution by assigning each station's monthly zonal wind to the nearest grid point without interpolation. When more than one station matched the same grid point, that grid point's value is estimated as the average of the available station values. Sub-sampling the CMIP3 models at the IGRA station locations yielded similar results, but sub-sampling decreases the ensemble mean jet displacement from $0.11 \pm 0.10^\circ$ per decade to $0.03 \pm 0.16^\circ$ per decade.

Our jet-based measure of tropical width is based on locating the 'sides' of the jet using the 75th percentile of monthly mean zonal wind for each tropospheric (850–300 hPa) pressure level[12]. The 75th percentile is estimated by sorting the monthly mean zonal wind—for each hemisphere and tropospheric pressure level—from low to high and taking the $0.75 \times (N+1)$ value, where N is the number of zonal wind values (that is, latitudes). Taking the midpoint and averaging over pressure levels yields a time series of monthly jet locations for each hemisphere.

Displacements for all metrics are estimated by first smoothing the zonal monthly mean of the appropriate field(s) and interpolating to 0.5° resolution using cubic splines. Smoothing was performed by taking a running mean over about 10° of latitude. However, nearly identical results are obtained without interpolating.

For trend uncertainty calculations (in the case of one observational metric), the influence of serial correlation is accounted for by using the effective sample size, $n(1-r_1)(1+r_1)^{-1}$, where n is the number of years and r_1 is the lag-1 autocorrelation coefficient[30].

When multiple realizations (or observational data sets for a given metric) are available, trend uncertainty is estimated as twice the standard error. These 2σ ranges are approximate, given that we have a ten-member ensemble and cannot confirm that the trends are Gaussian-distributed. However, ten ensemble members is relatively large for such a study and is the largest we could manage given the high computational costs of running nine forcing scenarios.

31. Adler, R. *et al.* The version-2 Global Precipitation Climatology Project (GPCP) monthly precipitation analysis (1979–present). *J. Hydrometeorol.* **4,** 1147–1167 (2003).
32. Durre, I., Vose, R. S. & Wuertz, D. M. Overview of the Integrated Global Radiosonde Archive. *J. Clim.* **19,** 53–68 (2006).
33. Kalnay, E. *et al.* The NCEP/NCAR 40-year reanalysis project. *Bull. Am. Meteorol. Soc.* **77,** 437–471 (1996).
34. Kanamitsu, M. *et al.* NCEP-DOE AMIP-II Reanalysis (R-2). *Bull. Am. Meteorol. Soc.* **83,** 1631–1643 (2002).
35. Uppala, S. *et al.* The ERA-40 re-analysis. *Q. J. R. Meteorol. Soc.* **131,** 2961–3012 (2005).
36. Rienecker, M. M. *et al.* MERRA: NASA's Modern-Era Retrospective Analysis for Research and Applications. *J. Clim.* **24,** 3624–3648 (2011).
37. Saha, S. *et al.* The NCEP Climate Forecast System Reanalysis. *Bull. Am. Meteorol. Soc.* **91,** 1015–1057 (2010).
38. Clement, A., Burgman, R. & Norris, J. R. Observational and model evidence for positive low-level cloud feedback. *Science* **325,** 460–464 (2009).
39. Rossow, W. B. & Schiffer, R. A. ISCCP cloud data products. *Bull. Am. Meteorol. Soc.* **72,** 2–20 (1991).
40. Rossow, W. B. & Schiffer, R. A. Advances in understanding clouds from ISCCP. *Bull. Am. Meteorol. Soc.* **80,** 2261–2287 (1999).
41. Jacobowitz, H. *et al.* The Advanced Very High Resolution Radiometer Pathfinder Atmosphere (PATMOS) climate data set: a resource for climate research. *Bull. Am. Meteorol. Soc.* **84,** 785–793 (2003).
42. Pavolonis, M., Heidinger, A. & Uttal, T. Daytime global cloud typing from AVHRR and VIRS: algorithm description, validation, and comparisons. *J. Appl. Meteorol.* **44,** 804–826 (2005).
43. Yu, L. & Weller, R. A. Objectively analyzed air-sea heat fluxes for the global ice-free oceans (1981–2005). *Bull. Am. Meteorol. Soc.* **88,** 527–539 (2007).